Surface Pressure and Mountain Drag for Transient Airflow over a Mountain Ridge

PETER R. BANNON AND JOSEPH A. ZEHNDER

Department of the Geophysical Sciences, The University of Chicago, Chicago, IL 60637

(Manuscript received 2 January 1985, in final form 30 May 1985)

ABSTRACT

The linear problem of rotating, stratified, adiabatic, hydrostatic, Boussinesq airflow over a mountain ridge is solved analytically for the case where the spatially uniform, normally incident airflow is the sum of a steady and sinusoidally varying component. The mountain generates a response at the fundamental frequency of the wind and all higher harmonics.

During flow acceleration, the evanescent (vertically decaying) modes deepen and broaden the high–low pressure asymmetry across the ridge and increase the mountain drag. In contrast, the evanescent modes for steady airflow produce only a symmetric mountain anticyclone that generates no drag. The influence of the acceleration is more pronounced for mesoscale and synoptic-scale ridges (i.e., ridges whose Rossby number is order unity or smaller) and when the fundamental period is near the inertial period.

The transience also amplifies the magnitude of the maximum wave drag over its value predicted from steady airflow theory using the instantaneous wind speed. The total acceleration reaction due to both evanescent and wave modes can be larger than this steady airflow drag.

1. Introduction

Queney (1948) pioneered the theoretical study of mountain wave dynamics with a linear analysis of the steady flow over a mountain ridge. His results emphasize the vertical propagation of the mountain's influence and the asymmetric surface pressure patterns that can arise through wave processes. Queney also noted the effect of rotation and of the quasi-static approximation on the flow response. Later Sawyer (1959) realized that such asymmetric pressure patterns indicate a mountain drag, and he calculated that this wave drag is comparable to surface friction. The Queney model agrees qualitatively with observations (Smith, 1982), but quantitatively the model greatly underestimates the magnitude and width of the high–low pressure pattern for mesoscale and synoptic-scale mountains. Gill (1982) provides a clear review of mountain wave dynamics.

The Queney model, and many others, typically assume that the incident flow field is steady. Observations suggest that this assumption might be a bad approximation. Some atmospheric examples of this can be found in Smith (1982, see Fig. 3) and Buzzi and Tibaldi (1977), both of which depict a cold front interacting with a mountain range (the European and New Zealand Alps, respectively); Fig. 8 of Smith depicts a typhoon crossing Taiwan in 23 hours. Other geophysical examples of transient flow interaction with topography are discussed by Bell (1975) and Fels (1977) for the ocean and Venusian tides, respectively.

The purpose of the present study is, therefore, to investigate the effect of transience of the incident wind on the flow excited by a mountain. Specifically we modify Queney's model to include a temporally varying incident wind that consists of a steady and one sinusoidally varying component. The analytic solutions indicate that flow transience can significantly alter the surface pressure pattern and mountain drag for ridges whose Rossby number is order one or less when the period of oscillation is about the inertial period or larger.

Section 2 describes the model physics and mathematical analysis. The method of solution follows Bell (1975), but unlike Bell we include a steady component to the incident wind, allow for rotational effects, and explicitly compute the surface pressure pattern and drag. Section 2c discusses the behavior of the solution in the high and low frequency limit and in the quasi-geostrophic limit. Section 3 briefly reviews the results for the case of steady airflow, and Sections 4 and 5 present results for transient airflow. This comparison highlights modification of the pressure and drag by the evanescent modes during flow acceleration and amplification of the wave drag by the transience.

2. The model

a. Formulation

We modify the well-known Queney (1948) problem to allow the spatially uniform incident wind to be a function of time. The model atmosphere is a stably stratified, inviscid, hydrostatic Boussinesq fluid on an f-plane Cartesian coordinate system (x, y, z). The basic state velocity field is a zonal wind of the form

$$U = U_0[1 + \Delta \cos(\omega t)], \tag{1}$$

and is the sum of a steady component of magnitude U_0 and a single oscillatory component of magnitude ΔU_0 and frequency ω. The nondimensional parameter Δ measures the relative amplitude of the oscillatory flow component compared to the steady component and can be of order unity or larger. The Appendix discusses the dynamics of the basic state.

This flow is incident on a mountain ridge whose profile $h(x)$ is

$$h(x) = \frac{h_0}{1 + (x/a)^2}, \tag{2}$$

where h_0 is the mountain height and a is its half-width. Figure 1 summarizes the model geometry and physics.

The mountain is assumed to act as a small perturbation to the basic state flow (1). The linearized dynamics of this perturbed adiabatic flow satisfy

$$u_t + Uu_x - fv = -p_x/\rho_0 \tag{3}$$

$$v_t + Uv_x + fu = 0 \tag{4}$$

$$0 = -p_z/\rho_0 - g\rho/\rho_0 \tag{5}$$

$$u_x + w_z = 0 \tag{6}$$

$$\rho_t + U\rho_x = (\rho_0 N^2/g)w \tag{7}$$

where (u, v, w) is the perturbation velocity, p and ρ are the perturbation pressure, and density fields, respectively, $-g\hat{z}$ is the acceleration due to gravity, ρ_0 is a reference density, f is the constant Coriolis parameter, and $N^2 = -(g/\rho_0)d\rho_S/dz$ is the square of the constant buoyancy frequency associated with the stable basic state density stratification ρ_S. Subscripts x, z, and t denote zonal, vertical, and temporal partial differentiation, respectively. By symmetry the perturbation is independent of y.

The set (3)–(7) yields a single equation for w:

$$(D^2 + f^2)w_{zz} + N^2 w_{xx} = 0 \tag{8}$$

where the operator $D \equiv \partial/\partial t + U\partial/\partial x$ is a function of time. The kinematic boundary condition at the surface is, in linearized form,

$$w(x, z = 0, t) = Uh_x \tag{9}$$

while a boundedness or radiation condition holds at $z = +\infty$.

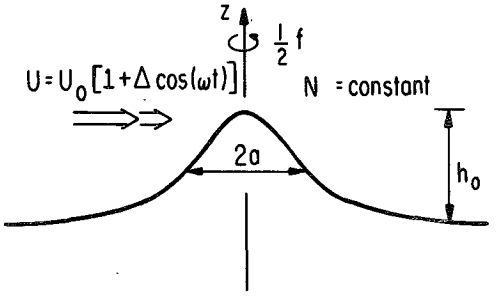

FIG. 1. A schematic illustration of the model. A zonal wind composed of a mean and periodic component with magnitudes U_0 and ΔU_0, respectively, is normally incident on a mountain ridge of height h_0 and halfwidth a centered at $x = 0$. The uniformly stratified model atmosphere lies on an f-plane, and linear dynamics is assumed.

b. Solution

To unravel the nonlinear time dependence inherent in (8), we follow Bell (1975) and introduce a horizontal coordinate ξ in a reference frame fixed with respect to the basic state flow (1), namely,

$$\xi \equiv x - \int_0^t U(t')dt', \quad \tau \equiv t \tag{10}$$

such that

$$\frac{\partial}{\partial \xi} = \frac{\partial}{\partial x}$$

$$\frac{\partial}{\partial \tau} = \frac{\partial}{\partial t} + U\frac{\partial}{\partial x}.$$

Then the inverse Fourier transform of w:

$$w(x, z, t) = \mathrm{Re}(2\pi)^{-1} \int \hat{w}(k, z, t) \exp(ikx)dk, \tag{11}$$

where a caret denotes a Fourier transform defined by

$$\hat{w}(k, z, t) = \int w(x, z, t) \exp(-ikx)dx, \tag{12}$$

may be written as

$$w(\xi, z, \tau) = \mathrm{Re}(2\pi)^{-1} \int \tilde{w}(k, z, \tau) \exp(ik\xi)dk, \tag{13}$$

where

$$\tilde{w}(k, z, \tau) = \hat{w}(k, z, \tau) \exp\left[ik \int_0^\tau U(t')dt'\right] \tag{14}$$

is the Fourier transform of w with respect to ξ-space. Here Re denotes the real part, and the limits of integration are assumed to be from $-\infty$ to $+\infty$ unless otherwise indicated. Taking the Fourier transform of (8) and (9) using (14) yields, respectively,

$$\left(\frac{\partial^2}{\partial \tau^2} + f^2\right)\tilde{w}_{zz} - N^2k^2\tilde{w} = 0, \tag{15}$$

$$\tilde{w}(k, 0, \tau) = \hat{h}(k)\frac{\partial}{\partial \tau}\left[\exp\left(ik \int_0^\tau U(t')dt'\right)\right] \tag{16}$$

where

$$\hat{h}(k) = h_0 \pi a \exp(-a|k|)$$

is the Fourier transform of the mountain profile $h(x)$. We note that (15) and (16) hold for arbitrary $U(t)$. For that given by (1), (16) becomes

$$\tilde{w}(k, 0, \tau) = \hat{h}(k) \frac{\partial}{\partial \tau} \exp[i(kU_0/\omega)(\omega\tau + \Delta \sin\omega\tau)] \tag{17}$$

or

$$w(k, 0, \tau) = \hat{h}(k) \sum_{n=-\infty}^{+\infty} i(-1)^n (kU_0 - n\omega) \times \exp[i(kU_0 - n\omega)\tau] J_n(\Delta k U_0/\omega) \tag{18}$$

using the identity (e.g., Abramowitz and Stegun, 1964)

$$\exp[ir \sin\alpha] = \sum_{n=-\infty}^{+\infty} (-1)^n \exp(-in\alpha) J_n(r), \tag{19}$$

where $J_n(r)$ is the nth order Bessel function of the first kind with argument r. The vertical structure of $\tilde{w}$ is determined from (15). The solution is

$$\tilde{w}(k, z, \tau) = \sum_{n=-\infty}^{+\infty} i(-1)^n (kU_0 - n\omega) \exp[im_n z + i(kU_0 - n\omega)\tau] \hat{h}(k) J_n(\Delta k U_0/\omega) \tag{20}$$

where

$$m_n^2 = k^2 N^2/[(kU_0 - n\omega)^2 - f^2]. \tag{21}$$

Choice of the sign of the vertical wavenumber m_n is based on either the boundedness or radiation condition at $z = \infty$. Evanescent modes with $m_n^2 < 0$ occur for k

$$k_- \equiv -k_f + nk_W < k < +k_f + nk_W \equiv k_+ \tag{22}$$

where $k_f = f/U_0$ and $k_W = \omega/U_0$. To ensure that the evanescent mode is bounded at $z = +\infty$, we choose the positive root of the imaginary wavenumber. Wave modes with $m_n^2 > 0$ occur for k

$$k > k_+ \quad \text{or} \quad k < k_-. \tag{23}$$

To ensure that the wave mode propagates energy upward at $z = +\infty$, we choose $\text{sgn}(m_n) = \text{sgn}(k - nk_W)$.

Although the mathematical problem is in terms of the vertical velocity, we focus our interest on the surface pressure field and associated mountain drag. Elimination of ρ from (5) and (7) yields

$$Dp_z = -\rho_0 N^2 w, \tag{24}$$

which may be transformed to

$$\frac{\partial}{\partial \tau} p_z = -\rho_0 N^2 w. \tag{25}$$

Hence one finds

$$\tilde{p}(k, z, \tau) = +\rho_0 N^2 \sum_{n=-\infty}^{+\infty} i(-1)^n \exp[im_n z + i(kU_0 - n\omega)\tau] m_n^{-1} \hat{h}(k) J_n(\Delta k U_0/\omega) \tag{26}$$

and the solution in physical space is

$$p(x, z, t) = \rho_0 N U_0 h_0 \sum_{n=-\infty}^{+\infty} \text{Re}(i/2)(-1)^n \times \int \exp(i\phi_n) \exp(-|\kappa|) \mu_n^{-1} J_n(\Delta\kappa/\kappa_W) d\kappa, \tag{27}$$

where the nondimensional parameters

$$\kappa = ka, \quad \kappa_W = \omega a/U_0, \quad \kappa_f = fa/U_0,$$
$$\mu_n^2 = U_0^2 m_n^2/N^2 = \kappa^2/[(\kappa - n\kappa_W)^2 - \kappa_f^2]$$
$$\phi_n = \kappa[x/a - (\Delta/\kappa_W) \sin\omega t] + m_n z - n\omega t \tag{28}$$

and the Fourier transform of the mountain profile have been introduced.

The term $-n\omega t$ in the expression for the phase function ϕ_n suggests that the mountain excites a response at the fundamental frequency of the incident wind and at all its harmonics as well as a steady response. However, the term in square brackets for ϕ_n indicates that the horizontal symmetry axis of each mode is $x = (a\Delta/\kappa_W) \sin(\omega t)$ and varies sinusoidally at the fundamental frequency and directly with the magnitude Δ of the oscillatory wind component. Thus even the "steady" $n = 0$ term undergoes an oscillation in time.

The inverse Fourier transforms in (27) are divided into three integrals, one over the range corresponding to (22) for the evanescent modes and two over the ranges (23) for the wave modes, that are evaluated numerically using Gaussian quadrature. Results of this integration appear in Sections 3–5.

c. *Limiting behavior of the solution*

In order to check the analysis and provide insight into the physics of the solution, we explore here the structure of the solution in various limits. For example, it is readily shown that our solution is consistent with that of Bell (1975). In Bell there is no steady wind component, so we take the limit $U_0 \to 0$ with ΔU_0 fixed. Then (20) and (21) become

$$\tilde{w}(k, z, \tau) = \sum_{n=-\infty}^{+\infty} (-1)^n (-in\omega) \times \exp[i(m_n z - n\omega\tau)] \hat{h}(k) J_n(\Delta k U_0/\omega)$$
$$m_n^2 = k^2 N^2/(n^2\omega^2 - f^2). \tag{29}$$

Noting that $J_{-n}(r) = (-1)^n J_n(r)$, these expressions in the absence of rotation reduce to the hydrostatic form of Bell's analysis.

Two limits to a steady state are possible. The first lets the oscillatory component of the incident wind vanish by setting $\Delta = 0$ in (27). This limit agrees with steady state theory for an incident wind of amplitude U_0. Section 4 discusses the properties of this solution.

Alternatively one can approach a steady state in the

limit of vanishing frequency $\omega \to 0$. Then by (1) the solution should reduce to that for steady state theory for an incident wind of amplitude $U_0(1 + \Delta)$. To show this we follow Bell (1975, p. 714) and utilize the integral representation of the Bessel function

$$J_n(r) = (1/2\pi) \int_{-\pi}^{+\pi} \exp[ir \sin\psi - in\psi]d\psi. \quad (30)$$

Then (27) can be rewritten as

$$p(x, z, t) = \rho_0 N U_0 h_0 \, \mathrm{Re}(i/2) \times \int d\kappa \sum_{n=-\infty}^{+\infty} \exp[i(\kappa x/a + m_n z)] \exp(-|\kappa|)\mu_n^{-1} I_n \quad (31)$$

where

$$I_n = \left(\frac{1}{2T}\right) \int_{-T}^{+T} \exp[i\kappa X/a + in\omega(t' - t)]dt' \quad (32)$$

$$X(t', t) = \int_t^{t'} [U(t'') - U_0]dt'' \quad (33)$$

and $T = \pi/\omega$. As $\omega \to 0$, $U(t) \to U_0(1 + \Delta)$ and $X \to \Delta U_0(t' - t)$. Then I_n becomes (e.g., Mathews and Walker, 1970, p. 100)

$$I_n \to \delta_{nn'} \exp[-i\omega t(n - n')] \quad (34)$$

where δ is the Kronecker delta function and $n' = -\Delta\kappa/\kappa_W$. Thus only the $n = n'$ term contributes in the series of (31), and the pressure field reduces to

$$p(x, z, t) = \rho_0 N U_0 h_0 \, \mathrm{Re}(i/2) \times \int d\kappa \exp(i\kappa x/a + imz) \exp(-|\kappa|)/\mu \quad (35)$$

where

$$\mu^2 = \frac{U_0^2 m^2}{N^2} \frac{\kappa^2}{\kappa^2(1 + \Delta)^2 - \kappa_f^2}.$$

It can be shown that this result is identical to the steady solution with incident wind $U_0(1 + \Delta)$.

In contrast, the argument of the Bessel function in the high frequency case is small so one can use the well-known approximation

$$J_n(r) = \frac{1}{n!}\left(\frac{r}{2}\right)^n \quad \text{for} \quad r \ll 1. \quad (36)$$

In the limit as $\omega \to \infty$, the Bessel function argument $\Delta\kappa/\kappa_W \to 0$. Since $J_n(0) = 1(0)$ for $n = 0$ ($n > 0$), only the $n = 0$ term contributes to the sum, and (27) becomes

$$p(x, z, t) = \rho_0 N U_0 h_0 \, \mathrm{Re}(i/2) \int d\kappa \exp(-|\kappa|) \times \exp(i\kappa x/a + im_0 z)/\mu_0. \quad (37)$$

As this result is identical to the steady solution with incident wind U_0, the transience has no effect on the pressure field in the high frequency limit.

Lastly we note that the solution (27) reduces to that for quasi-geostrophic theory. In the limit $\kappa_f \gg \kappa$ and $\kappa \gg n\kappa_W$,

$$\mu_n^2 \to -\kappa^2/\kappa_f^2 \quad (38)$$

and, upon substituting into (27),

$$p(x, z, t) = \rho_0 N U_0 h_0 \kappa_f \, \mathrm{Re}(1/2) \int d\kappa \exp(-|\kappa|) \times \exp[i(\kappa x/a - (\Delta\kappa/\kappa_W)\sin\omega t + i|\kappa|\hat{z})]S/|\kappa| \quad (39)$$

where $\hat{z} = Nz/U_0\kappa_f = (N/fa)z$ and

$$S = \sum_{n=-\infty}^{+\infty} (-1)^n \exp(-in\omega t) J_n(\Delta\kappa/\kappa_W) = \exp[i(\Delta\kappa/\kappa_W)\sin\omega t]$$

using (19). Thus (39) becomes

$$p(x, z, t) = \rho_0 fa N h_0 \left(\frac{1}{2}\right) \times \int d\kappa \exp[-(1 + \hat{z})|\kappa|] \cos(\kappa x/a)/|\kappa| \quad (40)$$

which is identical to the steady quasi-geostrophic result. Note that this solution consists solely of evanescent modes and is independent of the amplitude of the incident wind.

3. Surface pressure and mountain drag for steady airflow

We review here some salient results for steady airflow to provide a reference point for the transient results of the next sections. For steady flow, $\Delta = 0$, and only the $n = 0$ term contributes to the sum (27) that reduces to (37). The total field is the sum of evanescent and wave contributions (denoted with subscripts E and W), which at the surface are

$$p_E(x, 0) = \rho_0 N U_0 h_0 \times \int_0^{\kappa_f} \kappa^{-1} \exp(-\kappa)(\kappa_f^2 - \kappa^2)^{1/2} \cos(\kappa x/a)d\kappa \quad (41)$$

$$p_W(x, 0) = -\rho_0 N U_0 h_0 \times \int_{\kappa_f}^{\infty} \kappa^{-1} \exp(-\kappa)(\kappa^2 - \kappa_f^2)^{1/2} \sin(\kappa x/a)d\kappa \quad (42)$$

where we have used (22) and (23) and the symmetry of the integrals. Note that p_E is an even function of x that vanishes as $\kappa_f \to 0$ while p_W is an odd function that vanishes as $\kappa_f \to \infty$. (Here $\kappa_f = fa/U_0$ is a measure of the strength of the rotation and is the inverse of the Rossby number $\epsilon = U_0/fa$.)

Figure 2 plots the surface pressure field for the nonrotating case and for the rotating case with $\epsilon = 1$. These

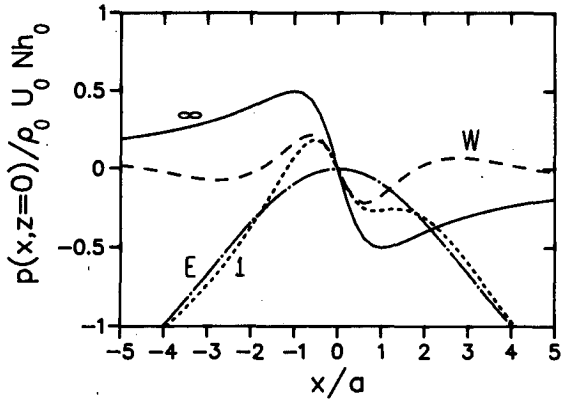

FIG. 2. Surface pressure field for steady ($\Delta = 0$) airflow as a function of x for the rotating case with Rossby number $\epsilon = U_0/fa = 1$ and for the nonrotating case ($\epsilon = \infty$). The dash curve labeled W is the antisymmetric component of the rotating case and is generated by the wave modes. The dash–dot curve labeled E is the evanescent component.

results are identical to Queney (1948). For typical atmospheric values of $\rho_0 = 1$ kg m^{-3}, $U_0 = 10$ m s^{-1}, $N = 10^{-2}$ s^{-1}, and $h_0 = 1$ km, the pressure scaling $\rho_0 U_0 N h_0$ is 1 mb. The nonrotating case exhibits an antisymmetric, upstream-high, downstream-low pattern with extrema halfway down the mountain at $x/a = \pm 1$ and a maximum pressure difference of 1 mb. This case consists entirely of wave modes.

The inclusion of rotation reduces the wave spectrum and creates an evanescent component. These evanescent modes produce a symmetric mountain anticyclone that has a logarithmic singularity that arises from the two-dimensional geometry. [Here the singularity is moved from $x = 0$ to infinity by replacing the cosine term in (41) with $\cos(\kappa x/a) - 1$. This approach, which amounts to adding a convenient constant to p, is also used in the transient case.] The wave component in the rotating case reveals smaller extrema located higher up the mountain than in the nonrotating case.

The mountain drag per unit length is

$$D = \int p(x, z = 0) \frac{\partial h}{\partial x} dx \tag{43}$$

and has a maximum value of $\frac{1}{4}\pi\rho_0 N U_0 h_0^2$ (Sawyer, 1959) for the nonrotating hydrostatic case, and decreases monotonically with increasing rotation (Smith, 1979). For example, the drag is $0.07\pi\rho_0 N U_0 h_0^2$ for $\epsilon = 1$. By symmetry the evanescent modes do not contribute to the drag. In the quasi-geostrophic limit (40), all the modes are evanescent, a symmetric anticyclone resides over the mountain, and there is no drag.

In summary, this review emphasizes that, for steady airflow, only the wave modes contribute to the pressure asymmetry across the mountain and to the mountain drag and that both asymmetry and drag decrease with increasing rotation.

4. Surface pressure for a transient airflow

For transient airflow, Δ is nonzero and all terms in the summation (27) contribute to the pressure field. At the surface the expressions for the evanescent and wave components may be written as, using (22), (23), and the symmetry of the integrands,

$$p_E(x, 0, t) = \rho_0 N U_0 h_0 \sum_{n=0}^{\infty} (-1)^n c_n \times \int_E |\mu_n|^{-1} \exp(-|\kappa|) \cos\theta J_n(\Delta\kappa/\kappa_W) d\kappa, \tag{44}$$

$$p_W(x, 0, t) = -\rho_0 N U_0 h_0 \sum_{n=0}^{\infty} (-1)^n c_n \times \int_W \mathrm{sgn}(\kappa - n\kappa_W)|\mu_n|^{-1} \exp(-|\kappa|) \sin\theta J_n(\Delta\kappa/\kappa_W) d\kappa, \tag{45}$$

respectively, where $c_n = 0.5$ (1.0) for $n = 0$ ($\neq 0$) and $\theta = \kappa x'/a - n\omega t$ with $x' = x - (\Delta a/\kappa_W)\sin\omega t$. In (44) the subscript E on the integral sign denotes the integral range $[\kappa_-, \kappa_+]$ where $\kappa_\pm = ak_\pm$; in (45) the corresponding subscript W is for the ranges $[-\infty, \kappa_-]$ and $[\kappa_+, \infty]$.

Plots (not shown) of the individual terms in (44) and (45) display a complex structure in space and time. The terms are oscillatory in the vicinity of the mountain but decay to zero in the farfield. (An exception is the evanescent $n = 0$ term which, like the steady case, possesses a logarithmic singularity.) In general, the horizontal structure increases as n increases, but the magnitude decreases. As noted earlier the symmetry axis is $x_S = a(\Delta/\kappa_W)\sin(\omega t)$ and is farthest upstream (downstream) of the mountain at $\omega t = -\pi/2(+\pi/2)$, corresponding to the time of maximum acceleration (deceleration). At $\omega t = 0$ the evanescent terms exhibit even, and the wave terms odd symmetry about this axis. In contrast, at $\omega t = -\pi/2$, the even-n evanescent terms and the odd-n wave modes exhibit even symmetry while the remaining terms possess odd symmetry.

As a specific example we present results for a strong periodic wind component ($\Delta = 1$) oscillating at the inertial period ($\omega = f$) that is incident on a mesoscale mountain range (steady Rossby number $\epsilon = 1$). Later we summarize the effect of variations in ϵ, ω and Δ. Figure 3 plots the net deviation of the surface pressure field from the steady airflow case for the evanescent (E), wave (W), and total ($T = E + W$) fields. The E and W curves are the sum of the first nine terms in (32) and (33), respectively, with the steady airflow case subtracted. At the time of maximum acceleration (Fig. 3a), the deviation consists of an essentially antisymmetric (about $x = 0$, the mountain peak) evanescent component with a broad upstream-high/downstream-low pattern and symmetric wave component with a ridge over the mountain. The total modification is asymmetric with a lee-side trough displaced downstream to $x/a \approx 3$.

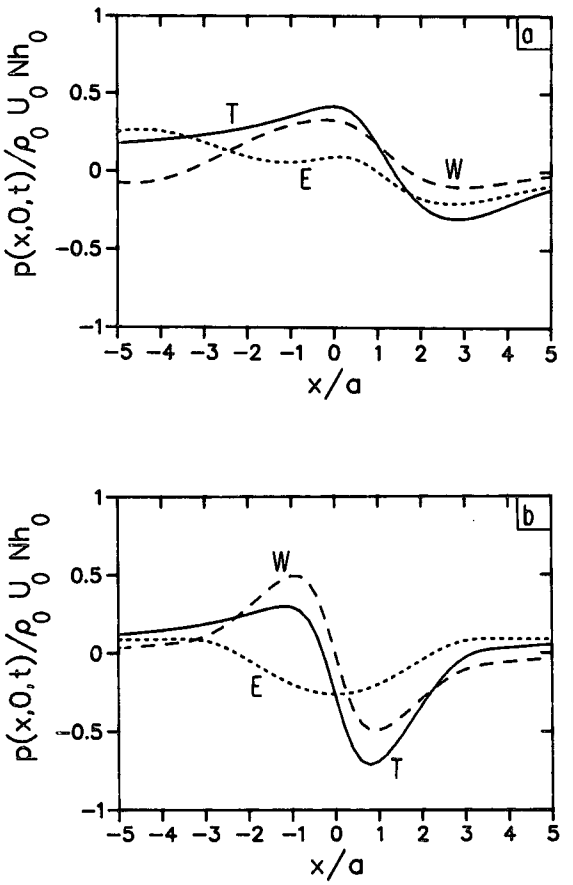

FIG. 3. Net deviation of the mountain induced surface pressure field from the steady airflow case as a function of x for the evanescent (E), wave (W), and total ($T = E + W$) fields with $\epsilon = 1$, $\Delta = 1$, and $\omega = f$ at the time (a) of maximum acceleration, $\omega t = -\pi/2$ and (b) of maximum wind, $\omega t = 0$.

At the time of maximum wind (Fig. 3b), the evanescent component is now symmetric with a trough over the mountain while the wave component is antisymmetric with an upstream-high/downstream-low pattern. The total deviation exhibits a 1.0 mb pressure difference across the mountain with a dominant lee-side trough.

Figure 4 summarizes the complete surface pressure field at critical times over the full cycle and compares it to the field predicted by steady airflow theory with the same instantaneous Rossby number, $\epsilon_i(t) = U_0[1 + \Delta \cos(\omega t)]/fa$. Again we set $\epsilon = 1$, $\Delta = 1$, and $\omega = f$. Figure 4a contrasts the response at times of maximum acceleration ($\omega t = -\pi/2$) and deceleration ($\omega t = +\pi/2$) when $\epsilon_i = \epsilon = 1$. The acceleration case exhibits a stronger upstream ridge and a stronger broader lee trough than that of steady airflow theory. The pattern during deceleration is similar to the steady one but includes a downstream ridge centered at $x/a = 4$.

Figure 4b presents the cases when the incident windspeed is an extremum. For maximum wind ($\omega t = 0$), the high–low pattern is similar to that (curve I) predicted by the steady airflow theory with $\epsilon_i = 2$, and the pattern is asymmetric with a more intense lee trough. (The asymmetry of curve I arises because it is the total pressure for $\epsilon_i = 2$ minus the steady anticyclone for $\epsilon = 1$.) At $\omega t = \pi$, the incident wind vanishes ($U = 0$), and steady airflow theory predicts no response. In contrast, the transient theory shows an upstream-low/downstream-high pressure pattern. In summary, Fig. 4 suggests that the pressure pattern can differ considerably from the steady results, but the transience does not significantly enhance the maximum cross-mountain pressure difference.

5. Mountain drag for a transient airflow

The contribution of the evanescent and wave modes to the mountain drag is found, from (27) and (43), to be

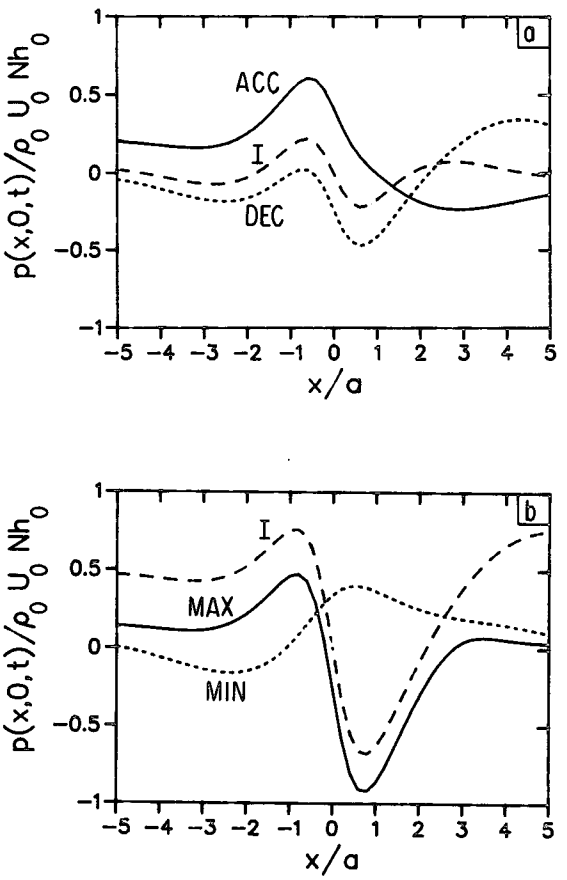

FIG. 4. Mountain induced surface pressure field as a function of x with $\epsilon = 1$, $\Delta = 1$, and $\omega = f$. In (a) curves ACC and DEC correspond to the times of maximum and minimum acceleration, $\omega t = -\pi/2$ and $+\pi/2$, respectively. In (b) curves MAX and MIN correspond to the times of maximum and minimum wind, $\omega t = 0$ and π, respectively. Curve I in (a) and (b) is the surface pressure field predicted from steady airflow theory using the instantaneous Rossby number $\epsilon_i = 1$ and 2, respectively. The steady mountain anticyclone for $\epsilon = 1$ is subtracted from each curve.

$$D_E(t) = \pi\rho_0 N U_0 h_0^2 \sum_{n=0}^{\infty} (-1)^{n+1} c_n \times \int_E |\mu_n|^{-1}\kappa \exp(-2|\kappa|) \sin\psi_n J_n(\Delta\kappa/\kappa_W) d\kappa \quad (46)$$

$$D_W(t) = \pi\rho_0 N U_0 h_0^2 \sum_{n=0}^{\infty} (-1)^n c_n \int_W \mathrm{sgn}(\kappa - n\kappa_W) \times |\mu_n|\kappa \exp(-2|\kappa|) \cos\psi_n J_n(\Delta\kappa/\kappa_W) d\kappa \quad (47)$$

where $\psi_n = (\Delta\kappa/\kappa_W)\sin\omega t + n\omega t$. Setting $\Delta = 0$ in (46) and (47) retrieves the steady airflow case (Smith, 1979).

In general the temporal structure (not shown) of the terms in (46) and (47) increase with n but decrease in magnitude. Note that the $n = 0$ terms have a time dependence due only to the lateral shift in the symmetry axis of the solution, while the higher-order terms augment this spatial oscillation with an amplitude oscillation. The evanescent terms exhibit odd symmetry with respect to the times of airflow extrema, $\omega t = 0$ and π, while the wave terms have even symmetry.

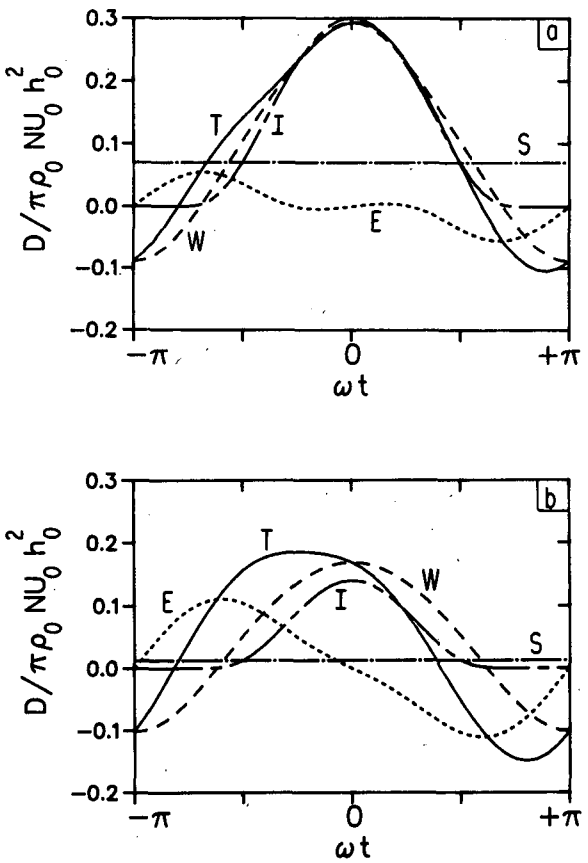

FIG. 5. Evanescent (E), wave (W), and total (T) drag as a function of time with $\Delta = 1$ and $\omega = f$ for (a) $\epsilon = 1$ and (b) $\epsilon = \frac{1}{2}$. Curves S and I are the drags predicted from steady airflow theory using the mean and instantaneous Rossby number, respectively.

The sum of the evanescent terms (Fig. 5a) generally contributes a positive drag during periods of acceleration, $-\pi < \omega t < 0$, and a negative one during deceleration, $0 < \omega t < \pi$. D_E vanishes in the absence of acceleration ($\omega t = 0, \pi$) and has an amplitude comparable to the drag D_S of steady airflow theory based on the mean wind speed U_0. Averaged over a complete cycle, D_E vanishes. The wave drag D_W is dominant and reaches a maximum at $\omega t = 0$ that is roughly four times D_S. This fourfold increase arises because: (i) the maximum wind is twice the mean wind (suggesting a doubling of the drag) and (ii) the instantaneous Rossby number of the mountain is twice that for the mean wind (suggesting enhanced excitation of wave modes). That the maximum D_W is slightly less than the drag D_I of steady airflow theory based on the instantaneous wind speed suggests that the steady theory is a relatively good approximation at the time of maximum wind. The total drag, $D_T = D_E + D_W$, is asymmetric about $\omega t = 0$ with larger values during acceleration and a minimum that precedes the time of minimum wind. The average total drag is identical to the average wave drag D_W, which is $0.10\pi\rho_0 N U_0 h_0^2$, compared to $0.07\pi\rho_0 N a_0 h_0^2$ for the steady flow and $0.11\pi\rho_0 N U_0 h_0^2$ for the instantaneous case D_I.

For a larger mountain (e.g., $\epsilon = \frac{1}{2}$; see Fig. 5b) the qualitative behavior of the drag is similar, but the relative importance of the evanescent component increases. This causes the maximum total drag to precede the maximum wind by about an eighth of a cycle. In addition, the maximum wave drag is slightly larger than that of D_I. The average value is 0.042, 0.0125, and $0.043\pi\rho_0 N U_0 h_0^2$ for the wave, steady, and instantaneous drag, respectively.

In summary the transience increases the average drag over that for steady flow. This behavior arises from the nonlinear dependence of the drag on the wind speed: the incremental increase in the drag during strong wind periods is larger than the decrease during weak wind periods. The average drag based on the instantaneous wind speed slightly overestimates this effect. In addition, the transience alters the drag at a given instant in time. For example, Fig. 5b at $\omega t = -\pi/2$ indicates about a twenty fold increase in the drag over either the steady or instantaneous results, and the evanescent component dominates the augmented wave component. The acceleration reaction is the difference between the total and instantaneous drag curves and is generally positive during accelerations. All the evanescent components contribute to the acceleration reaction while the difference, $D_W - D_I$, dictates the wave contribution.

Inspection of the drag formulae (46) and (47) indicates that, apart from the dimensional scaling factor $\pi\rho_0 N U_0 h_0^2$, the drag is a function of the three nondimensional parameters: Δ, ϵ and $\sigma = \omega/f$. (Note that $\kappa_f = \epsilon^{-1}$ and $\kappa_W = \sigma\kappa_f$.) Figure 6 indicates a monotonic but nonlinear increase in the effect of the transience

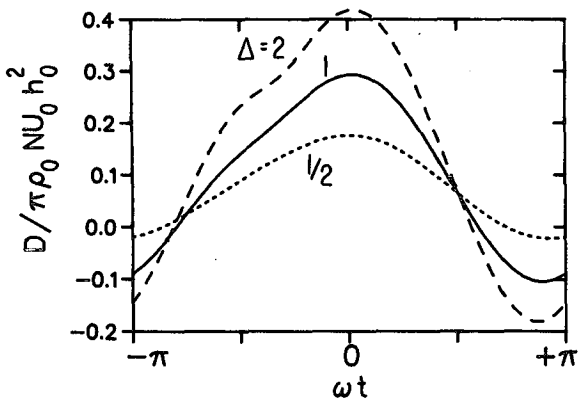

FIG. 6. Total drag as a function of time for various values of Δ. The solid curve is the reference case: $\epsilon = 1$, $\sigma = 1$, $\Delta = 1$.

as the magnitude of the oscillatory wind component increases. The dependence of the response on ϵ and σ is examined in Fig. 7 where the evanescent drag (at $\omega t = \pi/2$) and the wave drag (at $\omega t = -\pi/2$ and 0) for $\Delta = 1$ is plotted as a function of ω/f for various ϵ. In computing the curves in Fig. 7, the summation over n in (46) and (47) was terminated at $n = k$ once the kth term had a magnitude less than 10^{-5}. A minimum of 5 terms were included. For $\omega \leqslant 0.4f$ and $\epsilon = 2$ this criterion was not satisfied after 16 terms, and results are not plotted in Fig. 7c. It is seen that D_E ($\omega t = -\pi/2$) increases with decreasing ϵ and possesses a broad maximum. For $\epsilon < 1$ this maximum is centered near the inertial period case ($\omega = f$). In contrast D_W ($\omega t = -\pi/2$) decreases with increasing ϵ, but again the acceleration preferentially increases the drag for $\epsilon \leqslant 1$ with a maximum near the inertial period. At $\omega t = 0$, D_E vanishes, but D_W is nonzero. The transience significantly increases D_W for $\epsilon < 1$ and $\omega/f \geqslant 1$ but slightly decreases D_W for $\epsilon \geqslant 1$. The values for $\omega = 0$ in Fig. 7b and c differ because they correspond to the wave drag for steady airflow theory with $U = U_0$ and $2U_0$ respectively. This behavior is consistent with the low-frequency limit discussed in Section 2c. In the high-frequency limit [$\omega \to \infty$ and (37)], the curves in Fig. 7 will become asymptotic towards the steady drag for an incident wind speed of amplitude U_0.

6. Conclusions

The Queney model of airflow over a mountain ridge has been modified to include an oscillatory component to the incident wind. A formal series solution indicates that the mountain excites a response at the fundamental frequency of the inflow and at all its harmonics. No stationary response exists as the horizontal symmetry axis of each harmonic (including the $n = 0$ mode) shifts sinusoidally with time a distance $\Delta U_0/\omega$ from the mountain peak. The maximum upwind displacement occurs when the acceleration of the incident wind is a maximum. This lateral shift breaks the even symmetry about the mountain peak that the evanescent (vertically

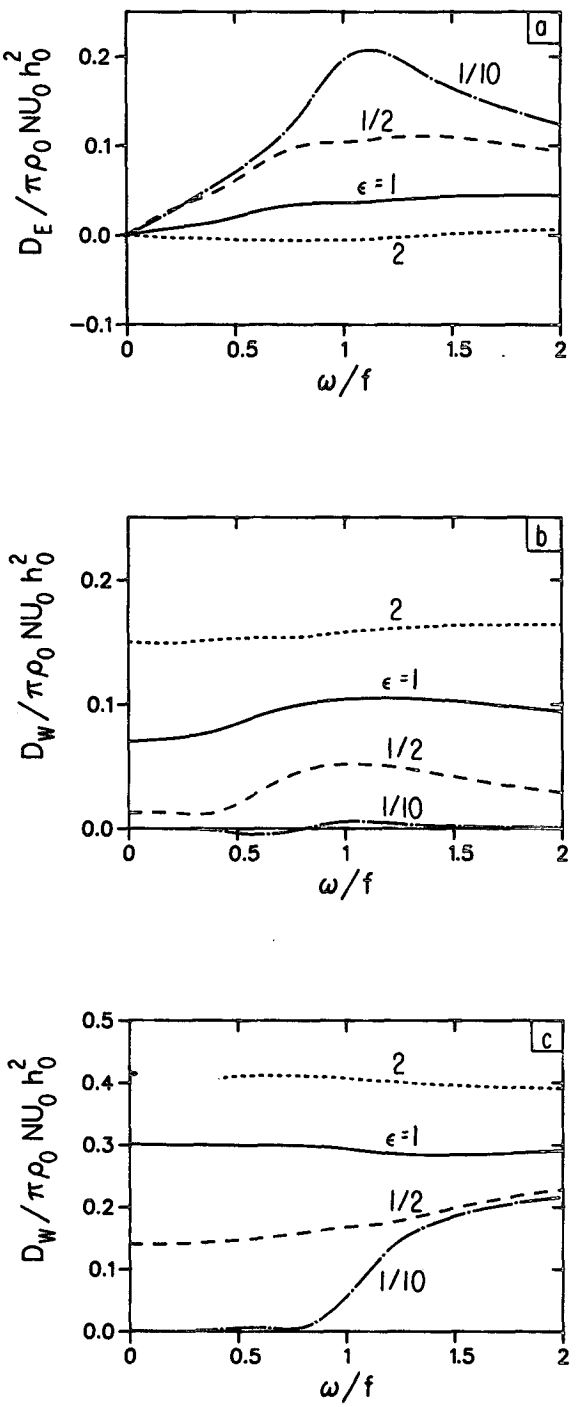

FIG. 7. Drag due to the (a) evanescent modes at $\omega t = -\pi/2$ and to the wave modes at (b) $\omega t = -\pi/2$, and (c) $\omega t = 0$ as a function of frequency with $\Delta = 1$ for various values of ϵ. Note that D_E ($\omega t = 0$) $\equiv 0$.

trapped) modes display for steady airflow and allows them to contribute to the mountain drag. Though the time-mean of this drag is zero, its instantaneous value can be comparable to the wave drag. In addition, by increasing the number of wave modes, the transience generally produces an enhanced wave drag. An extreme case of this effect is the presence of a negative drag when the incident wind is essentially zero (see Figs. 5 and 6). The effects of the transience are appreciable only for mountains where the Rossby number is order unity or smaller and when the period of oscillation is near the inertial period.

The present study has focussed on the surface pressure field and associated drag. The general solutions (20) and (27) can be used to examine the flow response of other variables and in the vertical. For example, by (5) the evanescent modes are associated with low-level density anomalies that are proportional to the pressure anomaly. Specifically the low-pressure evanescent surface pressure is shallow, warm-cored and, by (25), generated by subsidence.

Some model limitations suggest avenues of future research. Isolated topography rather than an infinitely long ridge should be examined to see if the resonance with any free topographic modes (e.g., Bannon, 1985) exist. Furthermore, isolated topography would enable two-dimensional incident flow $[U(t), V(t)]$ to be studied. Last we note that solutions with different time dependence can not be linearly superimposed. This shortcoming restricts direct application of the present results to observed case studies in the atmosphere where the incident windfield is not monochromatic in its temporal behavior. An alternative approach is the initial boundary value problem in which the zonal flow accelerates from an initial state of rest. The flow and wave fields in such a case may differ considerably from those during the accelerating phase of the oscillating wind problem presented here. Such a study would complement the present analysis and further our knowledge of transient airflow over topography.

Acknowledgments. Professor William Blumen referred us to the work of Bell (1975). Reviewer A encouraged the analysis of Section 2c. Financial support in part was provided jointly by the National Science Foundation (NSF) and the National Oceanic and Atmospheric Administration under NSF contracts ATM80-26790 and ATM84-02249.

APPENDIX

The Basic State Flow

The nonlinear, governing equations for the hydrostatic Boussinesq model are

$$\left.\begin{aligned} \frac{du}{dt} - fv &= -\frac{1}{\rho_0}\frac{\partial p}{\partial x}, \\ \frac{dv}{dt} + fu &= -\frac{1}{\rho_0}\frac{\partial p}{\partial y}, \\ 0 &= -\frac{1}{\rho_0}\frac{\partial p}{\partial z} - \frac{\rho g}{\rho_0}, \\ \frac{\partial u}{\partial x} + \frac{\partial v}{\partial y} + \frac{\partial w}{\partial z} &= 0, \\ \frac{d\rho}{dt} &= 0 \end{aligned}\right\} \quad \text{(A1)}$$

where ρ_0 is a constant reference density and

$$\frac{d}{dt} = \frac{\partial}{\partial t} + \frac{u\partial}{\partial x} + \frac{v\partial}{\partial y} + \frac{w\partial}{\partial z}.$$

A basic state velocity field consisting solely of a time dependent zonal wind, $U(t)$, is an exact solution of these equations provided the basic state pressure field p_s has the form

$$p_s = -\rho_0 \frac{\partial U}{\partial t} x - \rho_0 f U y - \int \rho_s g dz + p_{00} \quad \text{(A2)}$$

where p_{00} is a reference pressure and $\rho_s(z)$ is the stable basic state density field. The basic state is in hydrostatic balance in the vertical and in geostrophic balance in the meridional direction. A body force, given here by the zonal pressure gradient, provides the zonal acceleration of the flow. Addition of perturbation fields to this basic state and substitution into (A1) yields the set (3)–(7) upon linearization.

REFERENCES

Abramowitz, M., and I. A. Stegun, Eds., 1964: *Handbook of Mathematical Functions.* National Bureau of Standards, 1046 pp.

Bannon, P. R., 1985: Flow acceleration and mountain drag. *J. Atmos. Sci.*, **42,** 2445–2453.

Bell, T. H., 1975: Lee waves in stratified flows with simple harmonic time dependence. *J. Fluid Mech.*, **67,** 705–722.

Buzzi, A., and S. Tibaldi, 1977: Inertial and frictional effects on rotating and stratified flow over topography. *Quart. J. Roy. Meteor. Soc.*, **103,** 135–150.

Fels, S. B., 1977: Momentum and energy exchange due to orographically scattered gravity waves. *J. Atmos. Sci.*, **34,** 499–514.

Gill, A. E., 1982: *Atmosphere-Ocean Dynamics.* Academic Press, 662 pp.

Mathews, J., and R. L. Walker, 1970: *Mathematical Models of Physics* (2nd ed.). W. A. Benjamin, 501 pp.

Queney, P., 1948: The problem of air flow over mountains: A summary of theoretical studies. *Bull. Amer. Meteor. Soc.*, **29,** 16–26.

Sawyer, J. S., 1959: The introduction of the effects of topography into methods of numerical forecasting. *Quart. J. Roy. Meteor. Soc.*, **85,** 31–43.

Smith, R. B., 1979: The influence of the earth's rotation on mountain wave drag. *J. Atmos. Sci.*, **36,** 177–180.

——, 1982: Synoptic observations and theory of orographically disturbed wind and pressure. *J. Atmos. Sci.*, **39,** 60–70.